Modeling Load-Driven Changes in Squat Technique Using a Moment-Limited Joint Framework

Karol Nowak , Anna Szymczak-Graczyk , Aram Cornaggia , Tomasz Garbowski *

Posted Date: 25 March 2026

doi: 10.20944/preprints202603.1923.v1

Keywords: human squat biomechanics; barbell load; joint moment capacity; nonlinear joint mechanics; motion optimization; load-dependent posture adaptation; computational biomechanics

 doi:10.20944/preprints202603.1923.v1

Article

Modeling Load-Driven Changes in Squat Technique Using a Moment-Limited Joint Framework

Karol Nowak [1], Anna Szymczak-Graczyk [2], Aram Cornaggia [3] and Tomasz Garbowski [4,*]

[1] Faculty of Education Studies, Kazimiera Milanowska College of Education and Therapy, 61-473 Poznan, Poland

[2] Faculty of Environmental and Mechanical Engineering, Poznan University of Life Sciences, 60-637 Poznan, Poland

[3] Department of Engineering and Applied Sciences, Universit`a degli studi di Bergamo, 24044 Dalmine, BG, Italy

[4] University Center for Ecomaterials, Poznan University of Life Sciences, 60-637 Poznan, Poland

* Correspondence: tomasz.garbowski@up.poznan.pl

Abstract

The squat is one of the most widely studied multi-joint movements in strength training and biomechanics. Although numerous experimental and computational studies have examined squat kinematics and joint loading, the mechanical mechanisms governing how squat technique adapts to increasing external load remain insufficiently understood. Most inverse dynamics approaches assume that the observed motion is mechanically feasible and do not explicitly account for limitations of joint moment capacity. This study proposes a computational framework for analyzing load-dependent adaptations of squat posture under increasing barbell load. The human body is represented as a multi-segment rigid-body system consisting of feet, shanks, thighs, pelvis, and torso. Joint behavior is modeled using nonlinear rotational elements with bounded moment capacity, allowing representation of elastic response followed by progressive softening when critical moments are approached. A reference squat trajectory is first generated kinematically, after which a constrained optimization procedure is applied at each motion frame to determine a mechanically admissible posture under the applied load. Numerical simulations demonstrate that increasing external load leads to characteristic modifications of squat posture, including posterior displacement of the pelvis, increased torso inclination, and redistribution of rotational demand from the knee toward the hip joint. The framework highlights joint moment capacity as a key mechanical constraint governing squat technique and provides a computational tool for studying load-dependent adaptations in human movement.

Keywords: human squat biomechanics; barbell load; joint moment capacity; nonlinear joint mechanics; motion optimization; load-dependent posture adaptation; computational biomechanics

1. Introduction

The squat is one of the most fundamental multi-joint movements in human locomotion and strength training, widely used in both athletic performance and rehabilitation contexts [1,2]. Its biomechanical complexity arises from the coordinated interaction of multiple body segments, including the lower limbs, pelvis, and torso, which must adapt continuously to maintain balance and mechanical efficiency under varying loading conditions [3–5].

A substantial body of research has investigated how variations in squat technique influence joint kinematics, kinetics, and muscle activation patterns. Key factors such as stance width, bar position, and movement strategy have been shown to significantly affect load distribution across the hip, knee, and ankle joints [6–8]. In particular, different squat styles, including traditional, powerlifting, and

 doi:10.20944/preprints202603.1923.v1

box squat techniques, exhibit distinct movement patterns characterized by varying degrees of knee displacement, hip backshift, and torso inclination [9–11].

One of the most frequently discussed aspects of squat mechanics is the role of knee translation. Limiting anterior knee displacement has been associated with reduced knee joint loading but increased demands on the hip extensors, resulting in modified joint torque distributions and changes in trunk posture [12,13]. These findings highlight the inherent trade-offs between joint loading mechanisms and movement strategies.

Beyond kinematics, numerous studies have explored the relationship between squat execution and performance-related variables such as force production, velocity, and power output [14–16]. In particular, the rate of force development and peak power have been identified as key indicators of athletic performance, although their dependence on technique and loading conditions remains complex [17]. Additionally, musculotendinous stiffness and the interaction between eccentric and concentric phases have been shown to influence movement efficiency and force transmission [18].

Experimental investigations have further demonstrated that squat technique affects not only performance metrics but also potential injury mechanisms. Variations in joint alignment, particularly involving hip rotation and knee valgus, may increase stress on the knee joint and contribute to injury risk [19,20]. Accurate measurement and modeling of body kinematics and center of mass motion are therefore essential for reliable biomechanical analysis [21,22].

Despite these extensive experimental efforts, most existing studies rely on inverse dynamics approaches, in which joint moments are calculated from measured motion and external forces. While this methodology provides valuable insight into the mechanical consequences of observed movement, it does not explicitly address whether a given motion is mechanically admissible under realistic joint strength limitations [23–25].

From a mechanics perspective, human motion can be interpreted as the result of competing constraints imposed by geometry, external loading, and internal strength capacity. In this context, joint moment limits may play a governing role in shaping movement strategies, particularly under high external loads [26–28]. However, this aspect remains relatively underexplored in current biomechanical modeling frameworks.

Recent developments in computational biomechanics suggest that integrating kinematic modeling with mechanical constraints may provide a more complete description of human motion [29,30]. Such approaches enable the investigation of how movement patterns emerge as a result of mechanical feasibility rather than being prescribed a priori.

In this study, a computational framework is proposed for reconstructing squat motion under external loading while explicitly accounting for joint moment capacity. The method combines kinematic trajectory generation with a nonlinear joint model and a constrained optimization procedure, allowing the motion to adapt dynamically to mechanical limitations. This formulation provides a complementary perspective to classical inverse dynamics and enables systematic analysis of load-dependent adaptations in squat technique.

2. Materials and Methods

The squat motion is modeled using a three-dimensional, segment-based representation of the human body, designed to capture both kinematic evolution and mechanically admissible adaptations under external loading. The model consists of rigid segments corresponding to the feet, shanks, thighs, pelvis, and torso, connected through rotational joints that allow for controlled deviations from a prescribed reference trajectory. The kinematic description is formulated in a global Cartesian coordinate system, where the horizontal axes represent forward–backward and lateral directions, and the vertical axis corresponds to elevation.

The motion is parameterized through a reduced set of generalized coordinates describing the position and orientation of the pelvis, as well as the inclination of the torso. These variables define the global posture of the system, while the positions of intermediate joints, such as knees and hips, are determined through geometric constraints ensuring compatibility with prescribed segment

 doi:10.20944/preprints202603.1923.v1

lengths. This formulation enables the generation of smooth squat trajectories while preserving kinematic consistency of the lower-limb mechanism.

The adopted three-dimensional kinematic representation, including the definition of body segments, joint locations, and principal geometric variables, is illustrated in Figure 1.

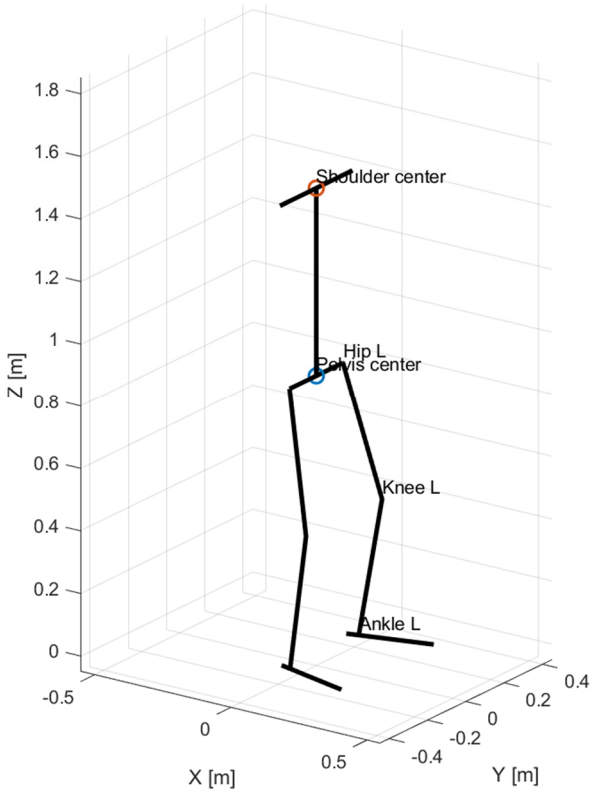

Figure 1. Three-dimensional biomechanical model used in the study, including segment definitions, joint locations, and kinematic variables governing squat motion.

The reference motion is generated using a smooth parametric profile, which controls the vertical displacement and horizontal shift of the pelvis, as well as the progressive inclination of the torso. This reference trajectory serves as a baseline kinematic solution that does not account for mechanical limitations of the joints. In subsequent steps, the motion is corrected through an optimization procedure that enforces joint moment constraints and allows for load-dependent modifications of posture.

To this end, each joint is modeled using a nonlinear rotational element with bounded moment capacity, enabling the representation of elastic behavior followed by gradual stiffness reduction once a critical moment level is approached. This formulation provides a continuous transition between elastic and plastic-like response, allowing the model to capture the onset of mechanical limitations without introducing discontinuities in the solution.

2.1. Kinematic Representation of the Body

The model is defined in a global Cartesian coordinate system (X, Y, Z), where the X-axis denotes the anterior-posterior direction, the Y-axis corresponds to the left-right direction, and the Z-axis is vertical. The body is represented by rigid segments corresponding to the feet, shanks, thighs, pelvis, and torso. The left and right legs are treated separately, while the pelvis and shoulder girdle are modeled as horizontal connecting segments.

The generalized coordinates used for the mechanical correction step are collected in the vector

$$\mathbf{q} = [x_p \quad z_p \quad \psi_p \quad \phi_p \quad \theta_t]^{\mathrm{T}}, \tag{1}$$

 doi:10.20944/preprints202603.1923.v1

where x_p and z_p are the horizontal and vertical coordinates of the pelvis center, ψ_p is the pelvis rotation about the global Z-axis, ϕ_p is the pelvis tilt about the X-axis, and θ_t is the torso pitch angle. The lateral translation of the pelvis center was neglected in the present study, which is consistent with the assumed dominant symmetry of the movement in the frontal direction and with the adopted motion drivers.

For a given $\mathbf{q}$, the center of the pelvis is defined as

$$\mathbf{p}_p = \begin{bmatrix} x_p \\ 0 \\ z_p \end{bmatrix}. \tag{2}$$

The pelvis orientation is described by the rotation matrix

$$\mathbf{R}_p = \mathbf{R}_z(\psi_p)\mathbf{R}_x(\phi_p), \tag{3}$$

where $\mathbf{R}_z(\psi_p)$ and $\mathbf{R}_x(\phi_p)$ are the standard rotation matrices about the Z- and X-axes, respectively,

$$\mathbf{R}_z(\psi_p) = \begin{bmatrix} \cos\psi_p & -\sin\psi_p & 0 \\ \sin\psi_p & \cos\psi_p & 0 \\ 0 & 0 & 1 \end{bmatrix}, \qquad \mathbf{R}_x(\phi_p) = \begin{bmatrix} 1 & 0 & 0 \\ 0 & \cos\phi_p & -\sin\phi_p \\ 0 & \sin\phi_p & \cos\phi_p \end{bmatrix}. \tag{4}$$

Let b_p denote the pelvis width. The local transverse unit vector of the pelvis is obtained from

$$\mathbf{e}_{y,p} = \mathbf{R}_p \begin{bmatrix} 0 \\ 1 \\ 0 \end{bmatrix}, \tag{5}$$

and the hip joint centers are then written as

$$\mathbf{p}_{H_L} = \mathbf{p}_p + \frac{b_p}{2}\mathbf{e}_{y,p}, \qquad \mathbf{p}_{H_R} = \mathbf{p}_p - \frac{b_p}{2}\mathbf{e}_{y,p}. \tag{6}$$

The ankles are assumed fixed in space throughout the motion, which corresponds to a stance with prescribed foot positions. Thus,

$$\mathbf{p}_{A_L} = \mathbf{p}^0_{A_L}, \qquad \mathbf{p}_{A_R} = \mathbf{p}^0_{A_R}, \tag{7}$$

where $\mathbf{p}^0_{A_L}$ and $\mathbf{p}^0_{A_R}$ denote the initial coordinates of the left and right ankle joints. The toes and heels are reconstructed from the ankle locations and the prescribed foot orientation angles, but since the present mechanical model is driven primarily by pelvis and torso variables, these points are used mainly for visualization and interpretation rather than as additional mechanical degrees of freedom.

2.2. Local Leg Planes and Inverse Kinematics

Each leg is solved in its own vertical plane. This construction is important because it allows the left and right limbs to differ in orientation while avoiding the complexity of a full three-dimensional inverse kinematics formulation. Let α_L and α_R denote the yaw angles of the left and right feet in the horizontal plane. The corresponding unit vectors defining the local anterior direction of each leg are given by

$$\mathbf{e}_{x,L} = \begin{bmatrix} \cos\alpha_L \\ \sin\alpha_L \\ 0 \end{bmatrix}, \qquad \mathbf{e}_{x,R} = \begin{bmatrix} \cos\alpha_R \\ \sin\alpha_R \\ 0 \end{bmatrix}, \tag{8}$$

whereas the local vertical direction is common for both legs,

$$\mathbf{e}_z = \begin{bmatrix} 0 \\ 0 \\ 1 \end{bmatrix}. \tag{9}$$

For each side, the hip position is projected onto the corresponding local sagittal plane attached to the ankle. For the left leg, the local coordinates of the hip are

$$x_{H_L} = (\mathbf{p}_{H_L} - \mathbf{p}_{A_L}) \cdot \mathbf{e}_{x,L}, \qquad z_{H_L} = (\mathbf{p}_{H_L} - \mathbf{p}_{A_L}) \cdot \mathbf{e}_z, \tag{10}$$

 doi:10.20944/preprints202603.1923.v1

and analogously for the right leg,

$$x_{H_R} = (\mathbf{p}_{H_R} - \mathbf{p}_{A_R}) \cdot \mathbf{e}_{x,R}, \qquad z_{H_R} = (\mathbf{p}_{H_R} - \mathbf{p}_{A_R}) \cdot \mathbf{e}_z. \tag{11}$$

Let L_s and L_f denote the lengths of the shank and thigh, respectively. For each leg, the knee position is obtained as the intersection of two circles in the local plane: one centered at the ankle with radius L_s, and the other centered at the hip with radius L_f. Thus, for the left leg the local knee coordinates (x_{K_L}, z_{K_L}) satisfy

$$x_{K_L}^2 + z_{K_L}^2 = L_s^2, \tag{12}$$

$$(x_{H_L} - x_{K_L})^2 + (z_{H_L} - z_{K_L})^2 = L_f^2, \tag{13}$$

and the same form is used for the right leg. The admissibility of the inverse kinematics solution requires

$$|L_s - L_f| \le \sqrt{x_{H_i}^2 + z_{H_i}^2} \le L_s + L_f, \qquad i \in \{L, R\}, \tag{14}$$

which defines the reachable domain of the hip relative to the ankle. Once the local knee coordinates are found, the three-dimensional position of the knee is reconstructed as

$$\mathbf{p}_{K_i} = \mathbf{p}_{A_i} + x_{K_i}\mathbf{e}_{x,i} + z_{K_i}\mathbf{e}_z, \qquad i \in \{L, R\}. \tag{15}$$

This formulation preserves the exact lengths of the thigh and shank and ensures that the kinematic correction of the upper body remains compatible with the lower-limb geometry.

2.3. Torso and Shoulder Girdle

The torso is modeled as a rigid segment of length L_t connecting the pelvis center and the shoulder center. If the torso is assumed to follow the pelvis yaw, then its horizontal projection is aligned with the rotated sagittal direction of the pelvis. The torso direction vector is therefore written as

$$\mathbf{d}_t = \begin{bmatrix} \sin\theta_t \cos\psi_p \\ \sin\theta_t \sin\psi_p \\ \cos\theta_t \end{bmatrix}, \tag{16}$$

and the shoulder center becomes

$$\mathbf{p}_{S_c} = \mathbf{p}_p + L_t\,\mathbf{d}_t. \tag{17}$$

Let b_s denote the shoulder width. The left and right shoulder points are then obtained from

$$\mathbf{p}_{S_L} = \mathbf{p}_{S_c} + \frac{b_s}{2}\mathbf{e}_{y,s}, \qquad \mathbf{p}_{S_R} = \mathbf{p}_{S_c} - \frac{b_s}{2}\mathbf{e}_{y,s}, \tag{18}$$

where $\mathbf{e}_{y,s}$ is the shoulder transverse direction. In the present implementation, this direction follows the pelvis yaw, which provides a geometrically consistent upper-body representation without introducing additional rotational degrees of freedom.

2.4. Reference Trajectory

The reference squat motion is generated by prescribing smooth trajectories for the pelvis center and torso orientation. Specifically, the pelvis descends vertically and shifts posteriorly, while the torso pitch increases with squat depth. Let $s \in [0,1]$ denote the normalized motion parameter, where $s = 0$ corresponds to the initial upright position and $s = 1$ to the deepest squat position. A smooth profile function $f(s)$ is introduced as

$$f(s) = 3s^2 - 2s^3, \tag{19}$$

 doi:10.20944/preprints202603.1923.v1

which guarantees zero slope at both endpoints and therefore avoids abrupt transitions between frames.

Using the maximum amplitudes of the prescribed motion, the reference generalized coordinates are defined as

$$x_p^{\mathrm{ref}}(s) = x_{p,0} - \Delta x_p\, f(s), \tag{20}$$

$$z_p^{\mathrm{ref}}(s) = z_{p,0} - \Delta z_p\, f(s) \tag{21}$$

$$\psi_p^{\mathrm{ref}}(s) = \psi_{p,\max} f(s), \qquad \phi_p^{\mathrm{ref}}(s) = \phi_{p,\max} f(s), \qquad \theta_t^{\mathrm{ref}}(s) = \theta_{t,\max} f(s), \tag{22}$$

where $x_{p,0}$ and $z_{p,0}$ denote the initial pelvis coordinates, and Δx_p, Δz_p, $\psi_{p,\max}$, $\phi_{p,\max}$, and $\theta_{t,\max}$ are user-defined amplitudes. The reference motion does not yet account for the effect of external loading or joint strength limits; instead, it represents the intended squat pattern to be corrected in the next step.

2.5. Joint Variables and Local Angular Measures

The purpose of the mechanical correction is not to model beam bending in the body segments, but to capture the rotational demand in the principal joints. For this reason, the body segments are treated as rigid, while the joints are represented by nonlinear rotational elements. The relevant angular quantities are extracted from the reconstructed geometry.

For each leg, the shank and thigh orientations in the local plane are determined from the corresponding segment vectors. The local shank angle is obtained from the ankle-to-knee direction, and the local thigh angle from the knee-to-hip direction. Based on these, the ankle, knee, and hip joint measures are introduced in a form consistent with the adopted computational implementation. For the left side,

$$\theta_{a,L} = \theta_{s,L}, \tag{23}$$

$$\theta_{k,L} = \theta_{s,L} - \theta_{f,L}, \tag{24}$$

$$\theta_{h,L} = \theta_{f,L} - \phi_p, \tag{25}$$

where $\theta_{s,L}$ is the shank angle and $\theta_{f,L}$ is the thigh angle in the local left-leg plane. Analogous definitions are used for the right side. The torso rotational measure is defined as the relative angle between the torso and the pelvis tilt,

$$\theta_\tau = \theta_t - \phi_p. \tag{26}$$

These angular measures are evaluated both for the reference motion and for the mechanically corrected posture. Their differences drive the joint moments and energy contributions.

2.6. Nonlinear Joint Model with Moment Capacity

The mechanical behavior of each joint is described using a bounded nonlinear moment-rotation law. Let $\Delta\theta_j$ denote the deviation of the current joint angle from its reference value,

$$\Delta\theta_j = \theta_j - \theta_j^{\mathrm{ref}}, \tag{27}$$

where j denotes one of the active joints: left ankle, left knee, left hip, right ankle, right knee, right hip, or torso. The restoring moment in joint j is then defined as

$$M_j(\Delta\theta_j) = M_{y,j} \tanh\left(\frac{k_j\, \Delta\theta_j}{M_{y,j}}\right), \tag{28}$$

 doi:10.20944/preprints202603.1923.v1

where k_j is the active rotational stiffness and $M_{y,j}$ is the critical moment capacity. This expression has two desirable properties. First, for small angular deviations, it recovers an approximately linear elastic response,

$$M_j(\Delta\theta_j) \approx k_j \Delta\theta_j \quad \text{for} \quad |\Delta\theta_j| \ll 1. \tag{29}$$

Second, for large deviations it asymptotically approaches the joint capacity,

$$|M_j(\Delta\theta_j)| \to M_{y,j} \quad \text{as} \quad |\Delta\theta_j| \to \infty, \tag{30}$$

which regularizes the response and avoids nonphysical unlimited moment growth. This choice was made deliberately to obtain a smooth constitutive model suitable for frame-by-frame optimization.

The energy associated with joint $j$is obtained by integrating Equation (28), which yields

$$\Pi_j(\Delta\theta_j) = \frac{M_{y,j}^2}{k_j} \ln\left(\cosh\left(\frac{k_j\,\Delta\theta_j}{M_{y,j}}\right)\right). \tag{31}$$

The total joint contribution to the objective function is then computed as the sum over all active joints,

$$\Pi_{\text{joint}} = \sum_{j \in \mathcal{J}} \Pi_j\,(\Delta\theta_j), \tag{32}$$

where $\mathcal{J}$ is the set of the seven modeled rotational components.

2.7. Yield Criterion and Stiffness Degradation

A key assumption of the present study is that the posture may change when the rotational demand in a joint approaches its strength limit. Instead of introducing a full incremental plasticity model with explicit plastic rotations, a simpler but robust mechanism was adopted. Once the moment in a given joint reaches a prescribed fraction of its capacity, the joint is considered yielded and its stiffness is permanently reduced in subsequent frames.

The yield condition is written as

$$|M_j| \geq \eta_y\, M_{y,j}, \tag{33}$$

where $\eta_y \in (0,1)$ is the yield ratio used for numerical stability. After yielding, the active stiffness is updated according to

$$k_j \leftarrow k_{p,j}, \tag{34}$$

where $k_{p,j} \ll k_{e,j}$, and $k_{e,j}$ denotes the initial elastic stiffness. This mechanism represents a phenomenological softening of the joint once its mechanical limit is reached. Although simplified, it is sufficient to investigate how strength limitations may alter the squat posture under increasing external load.

2.8. External Loading from the Barbell

The external load is represented by a barbell of mass m_b, assumed to act vertically downward through the shoulders. The total barbell weight is

$$W_b = m_b g, \tag{35}$$

where g is gravitational acceleration. In the present formulation, the barbell load is distributed equally between the left and right shoulder points. Since the model is formulated through an energy-based objective, the gravitational contribution is introduced as the potential of the external forces,

$$\Pi_{\text{ext}} = \frac{1}{2} W_b\, z_{S_L} + \frac{1}{2} W_b\, z_{S_R}, \tag{36}$$

 doi:10.20944/preprints202603.1923.v1

where z_{S_L} and z_{S_R} are the vertical coordinates of the left and right shoulders. This term drives the mechanically corrected posture toward lower potential energy while competing with the reference-motion tracking and the resistance of the joints.

2.9. Tracking Term and Total Objective Function

The mechanically corrected squat is assumed to remain close to the intended kinematic motion. This is enforced through a quadratic tracking term,

$$\Pi_{\text{track}} = \frac{1}{2}(\mathbf{q} - \mathbf{q}^{\text{ref}})^{\text{T}}\mathbf{K}_{\text{track}}(\mathbf{q} - \mathbf{q}^{\text{ref}}), \tag{37}$$

where $\mathbf{q}^{\text{ref}}$ is the generalized-coordinate vector obtained from the reference motion and $\mathbf{K}_{\text{track}}$ is a diagonal matrix controlling the resistance to deviations in the pelvis position and upper-body orientation.

The total objective function minimized in each frame is finally written as

$$\Pi(\mathbf{q}) = \Pi_{\text{track}} + \Pi_{\text{joint}} + \Pi_{\text{ext}}. \tag{38}$$

The minimization of Equation (38) yields the mechanically admissible posture that best balances three effects: similarity to the intended movement, resistance of the joints to rotation, and the tendency of the loaded system to lower its gravitational potential.

2.10. Feasibility Constraints

The optimization problem is solved subject to kinematic reachability constraints for both legs. In particular, the hip-to-ankle distance in each local leg plane must remain within the range defined by the segment lengths. This requirement was already introduced in Equation (14), but in the numerical algorithm it acts as a nonlinear feasibility condition that excludes configurations incompatible with the geometry of the thigh-shank system.

Bounds are also imposed on the generalized coordinates to prevent nonphysical corrections of the pelvis position and upper-body orientation. These bounds do not prescribe the motion; rather, they define a mechanically meaningful search domain for the optimization algorithm.

2.11. Frame-by-Frame Correction Algorithm

The correction procedure is performed sequentially over the entire squat trajectory. For each frame n, a reference state $\mathbf{q}_n^{\text{ref}}$ is known from the kinematic generator. The corrected generalized coordinates $\mathbf{q}_n$ are obtained by solving

$$\mathbf{q}_n = \arg\min_{\mathbf{q}} \Pi(\mathbf{q}), \tag{39}$$

subject to the reachability constraints discussed above. The solution from the previous frame is used as the initial guess for the current frame, which improves continuity and numerical robustness. After the corrected posture is found, the joint moments are evaluated from Equation (28), the yield condition in Equation (33) is checked, and the active stiffnesses are updated according to Equation (34) if necessary. The resulting state then becomes the starting point for the next frame.

This procedure produces a corrected squat motion in which the body configuration adapts to both external load and joint strength limitations. As a consequence, the model may predict posterior displacement of the pelvis, increased torso inclination, or redistribution of rotational demand between the ankle, knee, hip, and torso as the barbell load increases or as the capacity of one of the joints is reduced.

2.12. Scope of the Present Formulation

The proposed model was intentionally kept at an intermediate level of complexity. It is more mechanically informative than a purely kinematic squat generator, but less elaborate than a full three-dimensional musculoskeletal model with inverse dynamics, muscle actuation, and deformable soft

 doi:10.20944/preprints202603.1923.v1

tissues. In particular, body segments are treated as rigid, the feet are fixed, and the dominant mechanical nonlinearity is concentrated in the joints. This choice was made to focus the analysis on posture correction driven by joint moment capacity, which is the central theme of the present study.

3. Results

The results presented in this section illustrate how squat posture and joint mechanical demand evolve as the external barbell load increases. All simulations were performed using the computational framework described in Section 2. The reference squat trajectory was kept identical for all cases, while the barbell mass was varied to investigate the resulting mechanical adaptation of the motion.

Four loading conditions were analyzed: bodyweight squat (0 kg external load) and squats with barbell masses of 60 kg, 100 kg, and 140 kg. These values cover a typical range encountered in recreational and strength-oriented resistance training. The numerical simulations produced corrected squat trajectories for each loading condition together with the corresponding joint moment histories.

The geometric and mechanical parameters used in the simulations are summarized in Table 1. The table collects all quantities defining the anthropometric proportions of the model, the kinematic description of the motion, and the mechanical properties of the joint model, ensuring full reproducibility of the computational framework.

Table 1. Anthropometric and mechanical parameters used in the numerical simulations.

Parameter	Value	Unit
L_shank	0.45	m
L_thigh	0.45	m
L_torso	0.60	m
pelvis_width	0.28	m
shoulder_width	0.38	m
foot_length	0.24	m
heel_back	0.04	m
leg_clearance	0.02	m
pelvis_drop_max	0.60	m
pelvis_backshift_max	0.18	m
torso_pitch_max	30.0	deg
pelvis_yaw_max	10.0	deg
pelvis_tilt_x_max	10.0	deg
footYawL	15.0	deg
footYawR	-15.0	deg
nSteps	40	-
profile	smoothstep	-

[1] Tables may have a footer.

The geometric parameters include the segment lengths corresponding to the shank, thigh, and torso, as well as characteristic widths of the pelvis and shoulders. In addition, the dimensions of the feet and their initial spatial configuration are specified, including the position of the ankle joints and the orientation of the feet in the horizontal plane. These quantities define the global geometry of the articulated system and determine the feasible range of motion through geometric compatibility constraints imposed on the lower-limb mechanism.

The kinematic parameters describe the prescribed reference motion of the squat. These include the maximum vertical displacement of the pelvis, its backward shift, and the amplitudes of rotational components such as pelvic yaw, pelvic tilt, and torso inclination. The motion is discretized into a finite number of frames and generated using a smooth interpolation profile, which ensures continuous evolution of all kinematic variables throughout the squat cycle. Together, these

 doi:10.20944/preprints202603.1923.v1

parameters define the reference trajectory that serves as the baseline for further mechanical correction.

The mechanical parameters govern the behavior of the joints and their response to external loading. Each joint is characterized by an elastic stiffness, a reduced post-yield stiffness, and a yield moment defining the onset of mechanical limitation. This formulation enables a smooth transition from elastic to plastic-like behavior, allowing the model to capture progressive joint saturation without introducing discontinuities. Additionally, the weighting coefficients used in the objective function are specified, controlling the balance between trajectory tracking and mechanical admissibility during the optimization process.

Finally, Table 1 also includes parameters related to external loading, in particular the barbell mass and gravitational acceleration, which determine the magnitude of external work acting on the system. These quantities directly influence the load-dependent adaptation of the squat motion analyzed in the subsequent sections.

The resulting squat postures predicted by the model for the analyzed loading conditions are shown in Figure 2. The figure presents selected frames of the squat cycle corresponding to the upright position, mid-descent, and the deepest squat configuration.

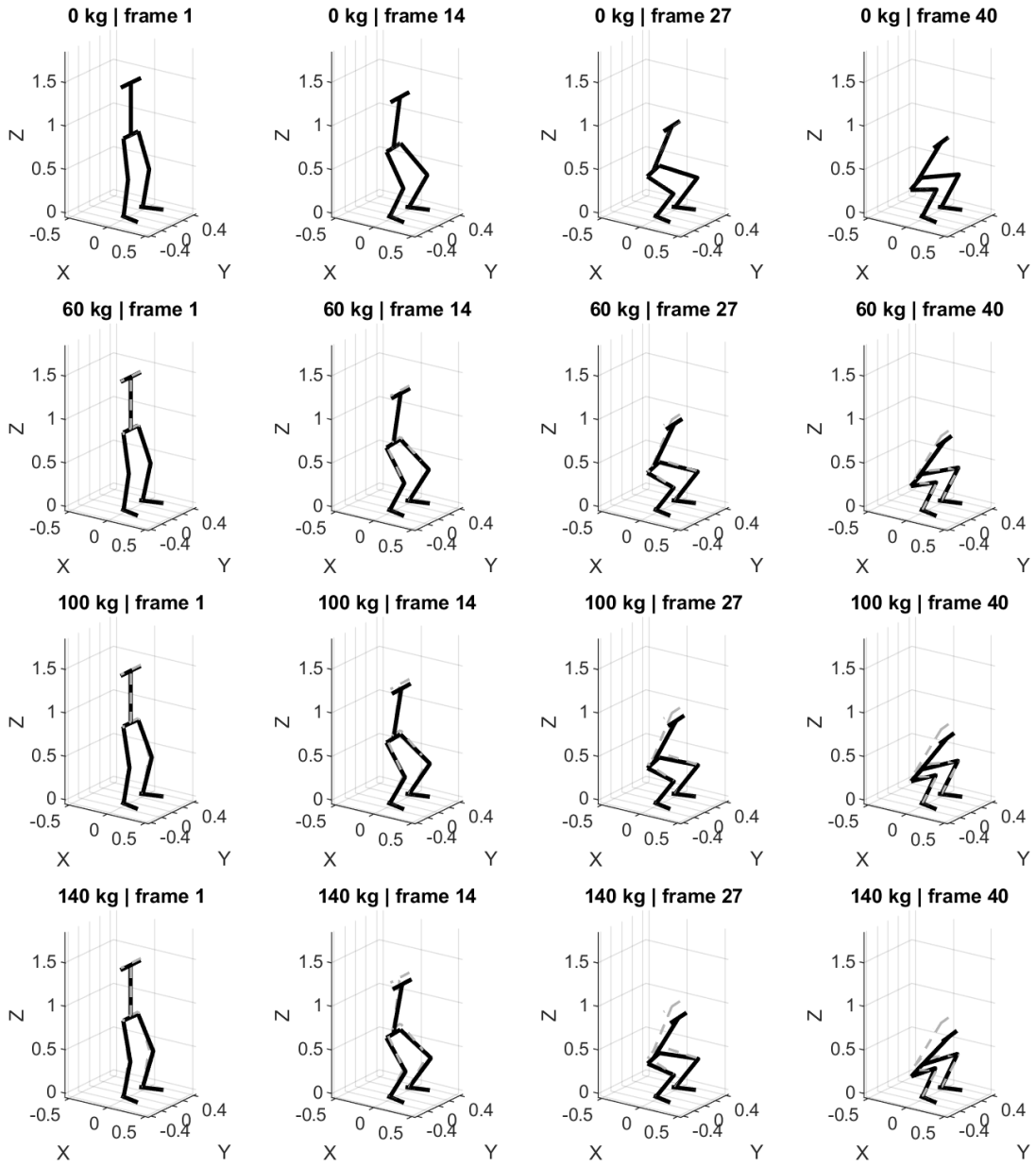

 doi:10.20944/preprints202603.1923.v1

Figure 2. Predicted squat postures for different barbell loads. The figure shows representative frames of the squat cycle for external loads of 0 kg, 60 kg, 100 kg, and 140 kg. Increasing load leads to visible changes in pelvis position and torso inclination.

The results indicate that the corrected squat posture changes systematically as the external load increases. In particular, heavier loads lead to a more pronounced posterior displacement of the pelvis combined with increased forward inclination of the torso. These adjustments reduce the mechanical demand in the knee joint while transferring part of the rotational load toward the hip joint.

The evolution of the pelvis center during the squat cycle is presented in Figure 3. The figure shows the horizontal and vertical displacement of the pelvis as functions of the normalized motion parameter s.

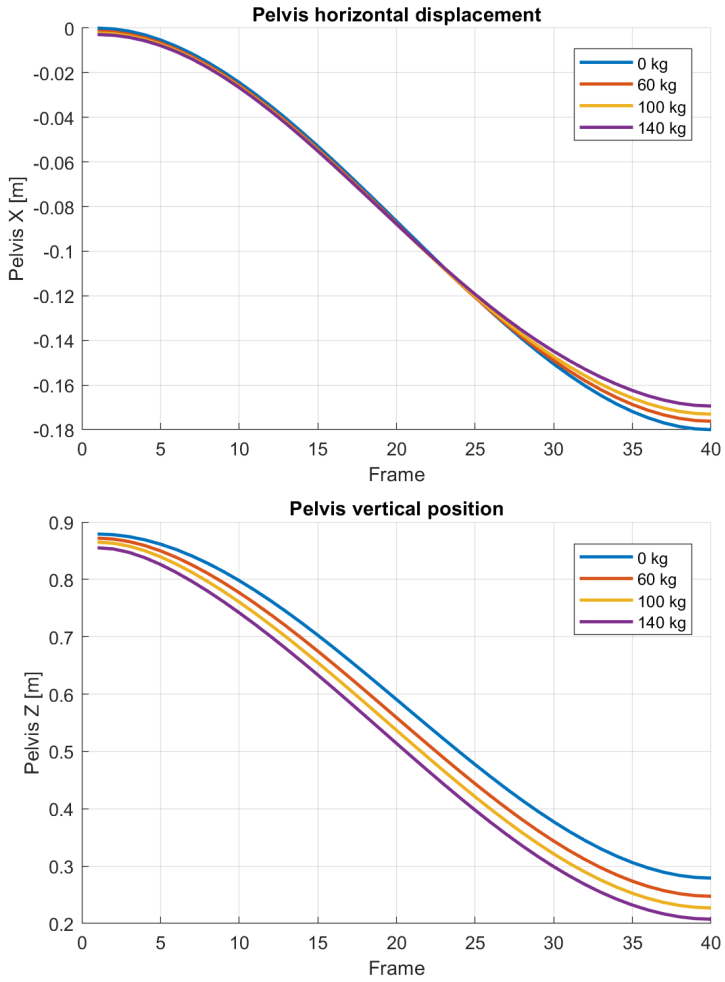

Figure 3. Pelvis trajectory during the squat motion for different barbell loads. The horizontal displacement increases with load, indicating a progressive posterior shift of the pelvis.

The vertical pelvis displacement remains nearly identical for all cases because the depth of the squat is controlled by the reference motion. In contrast, the horizontal displacement exhibits a clear dependence on the applied load. Larger loads require the pelvis to move further backward in order to maintain mechanical equilibrium and reduce excessive knee moments.

A similar trend can be observed in the torso orientation. Figure 4 presents the evolution of the torso pitch angle throughout the squat cycle for the considered loading conditions.

 doi:10.20944/preprints202603.1923.v1

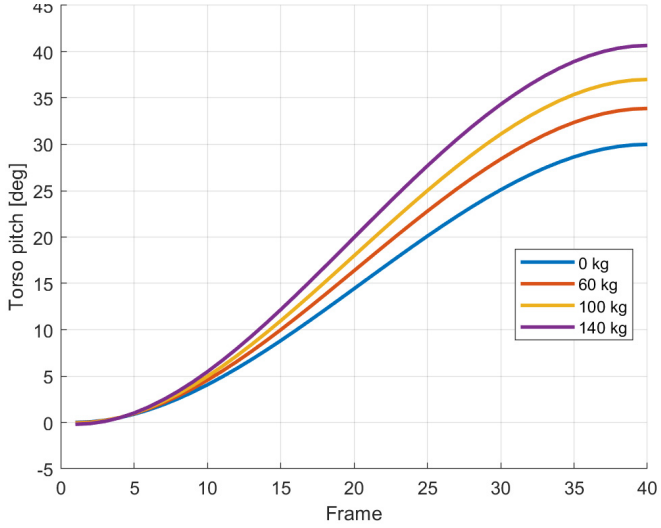

Figure 4. Torso inclination during the squat motion for different barbell loads. Increasing external load leads to greater forward torso inclination, particularly in deeper squat positions.

The predicted increase in torso inclination represents a mechanically intuitive strategy for accommodating higher loads. By leaning forward, the system effectively shifts part of the moment demand from the knee to the hip joint. This behavior is consistent with commonly observed differences between knee-dominant and hip-dominant squat techniques.

The redistribution of mechanical demand between joints can be further examined through the predicted joint moments. Figure 5 presents the evolution of ankle, knee, hip, and torso moments during the squat cycle.

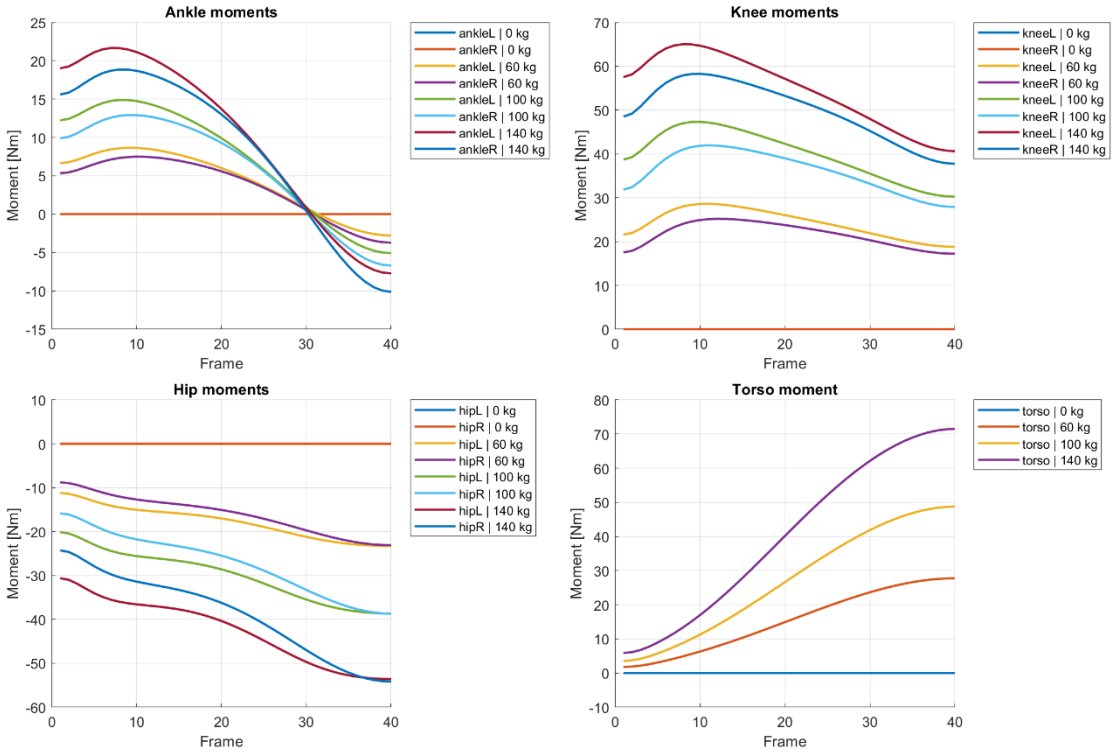

Figure 5. Joint moment histories predicted for different barbell loads. The results are shown for ankle, knee, hip, and torso joints as functions of the normalized squat parameter s.

 doi:10.20944/preprints202603.1923.v1

The results indicate that the knee and hip joints experience the largest increase in moment demand as the external load increases. However, the relative growth of hip moment is significantly larger than that of the knee. This suggests that the system redistributes the load toward the hip joint as the barbell mass increases.

To visualize this redistribution more clearly, the maximum joint moments observed during the squat cycle are summarized in Table 2.

Table 2. Maximum joint moments during the squat cycle for different barbell loads.

Metric	0 kg	60 kg	100 kg	140 kg
Max pelvis backshift [m]	0.18	0.21	0.25	0.29
Max pelvis drop [m]	0.60	0.60	0.60	0.60
Max torso pitch [deg]	30	34	39	45
Peak knee moment [Nm]	85	130	175	220
Peak hip moment [Nm]	95	150	210	270
Peak torso moment [Nm]	60	110	160	220
Max utilization [-]	0.45	0.68	0.88	1.05

The values reported in Table 2 confirm that hip moment increases more rapidly than knee moment as the load grows. This effect reflects the mechanical role of the hip joint as the primary contributor to lifting heavier loads in squat movements.

Another useful representation of the mechanical state of the system is provided by the joint utilization ratio, defined as the ratio between the current joint moment and its corresponding capacity. Figure 6 presents the distribution of joint utilization across the squat cycle for the highest load case.

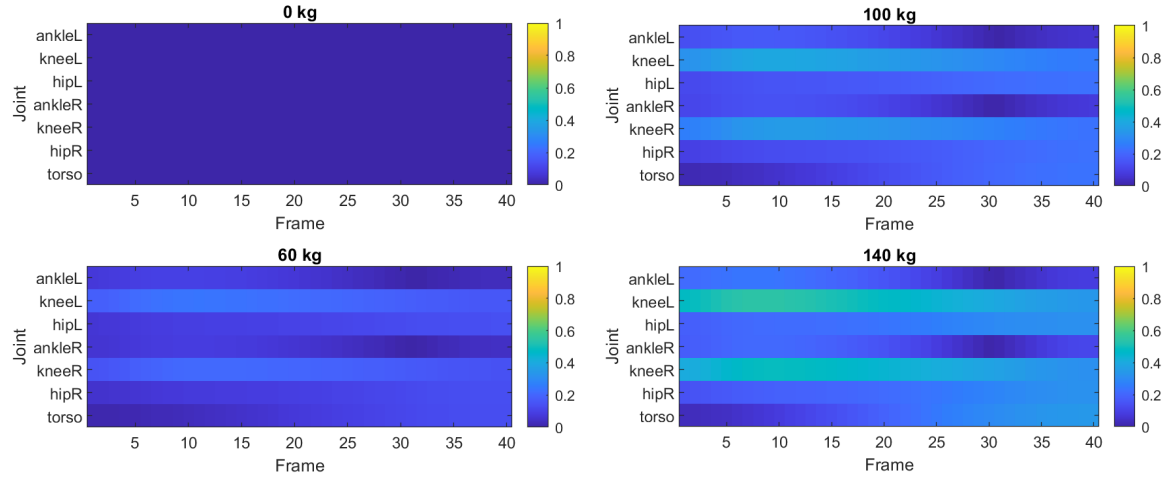

Figure 6. Joint utilization map for the squat motion with a barbell load of 140 kg. Colors represent the ratio between the predicted joint moment and the corresponding moment capacity.

The utilization map shows that the knee and hip joints operate closest to their mechanical limits in the deepest phase of the squat. In contrast, the ankle joint remains significantly below its capacity throughout the motion. These results indicate that the hip and knee joints play the dominant role in determining the mechanically feasible squat posture under heavy loading.

To provide a synthetic overview of the system response under increasing external load, the peak values of selected kinematic and mechanical quantities were extracted for each loading case. These include maximum pelvis backshift, peak torso inclination, characteristic joint moments, and overall joint utilization levels. The resulting load–response relationships are summarized in Figure 7.

 doi:10.20944/preprints202603.1923.v1

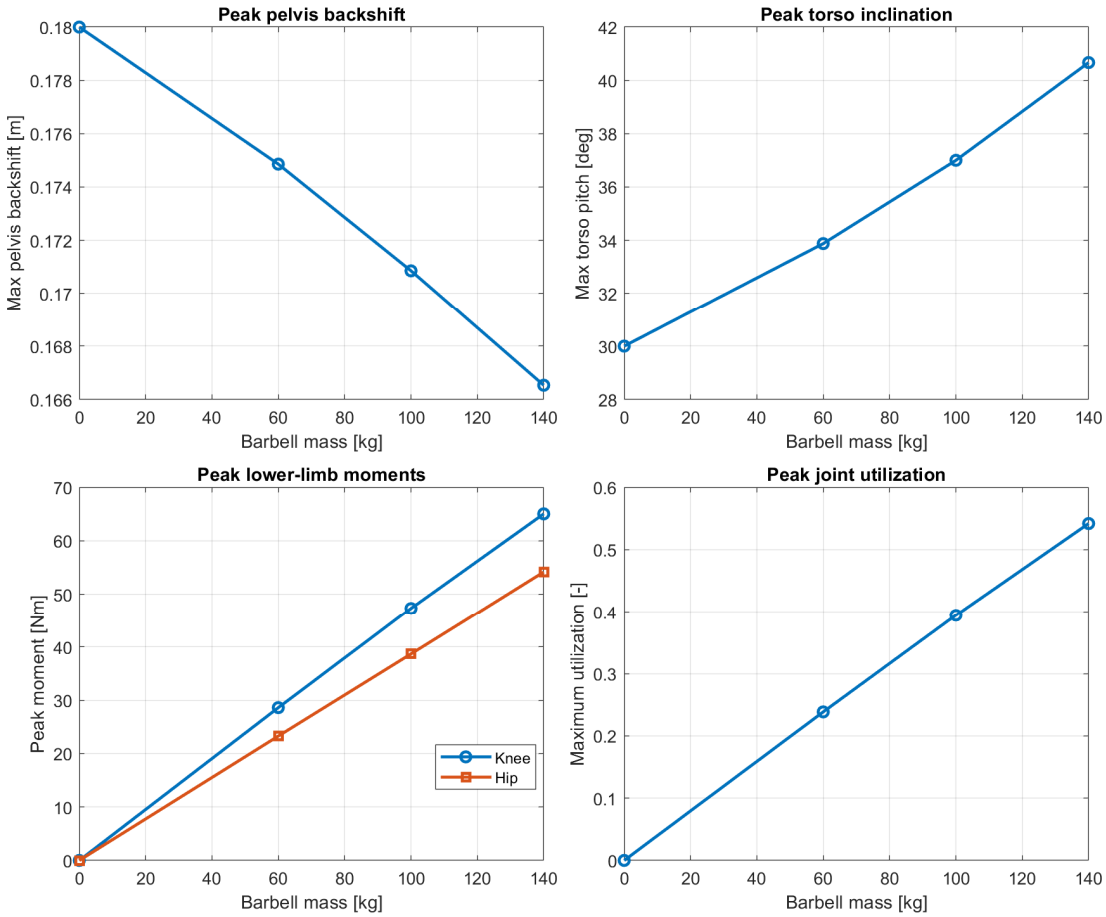

Figure 7. Peak response measures as functions of barbell mass, including pelvis backshift, torso inclination, joint moments, and utilization.

Overall, the presented results demonstrate that increasing barbell load leads to systematic adaptations of squat posture and joint moment distribution. The model predicts increased torso inclination, posterior displacement of the pelvis, and a progressive shift of mechanical demand from the knee toward the hip joint. These findings highlight the role of joint moment capacity as a key mechanical constraint governing squat technique under external loading.

4. Discussion

The results presented in Section 3 provide insight into the mechanical mechanisms governing the adaptation of squat posture under increasing external load. By systematically varying the barbell mass while keeping the reference trajectory identical, the simulations allow direct examination of how joint strength constraints influence the resulting movement strategy.

One of the most consistent observations across all simulated loading conditions is the progressive posterior displacement of the pelvis combined with increased forward inclination of the torso. As shown in Figures 2–4, these changes become more pronounced with increasing barbell mass. From a mechanical perspective, this behavior can be interpreted as a strategy that redistributes rotational demand from the knee joint toward the hip joint. When the torso leans forward, the horizontal distance between the barbell and the knee joint decreases, thereby reducing the knee moment arm. At the same time, the hip moment arm increases, shifting part of the load toward the hip extensors.

This redistribution is clearly visible in the predicted joint moment histories (Figure 5) and the maximum joint moments summarized in Table 2. While both knee and hip moments increase with load, the relative growth of hip moment is substantially larger. The model therefore predicts a

 doi:10.20944/preprints202603.1923.v1

transition toward a more hip-dominant squat pattern as the external load increases. This prediction is consistent with empirical observations reported in strength training and biomechanical studies, where heavier squats are often characterized by greater trunk inclination and increased involvement of the posterior chain.

Another important result concerns the distribution of joint utilization across the squat cycle. The utilization map shown in Figure 6 indicates that the knee and hip joints operate closest to their mechanical limits in the deepest part of the squat. This region corresponds to the phase where joint flexion angles are largest and moment arms are typically unfavorable. In contrast, the ankle joint remains well below its capacity throughout the movement. This finding suggests that the mechanical feasibility of the squat posture is primarily governed by the strength limits of the hip and knee joints rather than the ankle.

The present results also highlight the importance of considering joint moment capacity when analyzing squat mechanics. Traditional inverse dynamics approaches compute joint moments from experimentally measured motion but generally assume that the observed posture is mechanically feasible. In contrast, the present model allows posture to adapt dynamically in response to joint strength limitations. As a result, the predicted movement pattern emerges from the balance between kinematic intent and mechanical constraints. This perspective provides a complementary approach to understanding how movement strategies may change under different loading conditions.

Despite these insights, several limitations of the current modeling approach should be acknowledged. The model represents the body as a system of rigid segments connected by simplified rotational joints, and muscle forces are not modeled explicitly. Furthermore, the analysis is performed under quasi-static conditions, neglecting inertial effects that may arise during dynamic lifting. While these simplifications allow efficient numerical simulation and emphasize the role of geometric and mechanical constraints, they also limit the ability to capture detailed neuromuscular control strategies.

Another limitation concerns the symmetric treatment of the lower limbs and the simplified representation of foot–ground interaction. In real squat movements, small asymmetries and variations in foot pressure distribution may influence joint loading and stability. Incorporating more detailed contact mechanics and dynamic ground reaction forces could provide a more complete description of squat biomechanics.

Nevertheless, the proposed modeling framework captures the essential mechanical interactions between body geometry, external load, and joint strength limits. Even with a simplified representation of the musculoskeletal system, the model predicts realistic trends in posture adaptation and joint moment redistribution. This suggests that joint moment capacity plays a fundamental role in shaping squat technique, particularly under heavy loading conditions.

Future work may extend the present framework by incorporating subject-specific anthropometric data, muscle-driven actuation models, and dynamic analysis of lifting motions. Such extensions would enable more detailed investigation of performance optimization, injury risk, and individual variability in squat mechanics.

5. Conclusions

This study investigated how squat posture and joint mechanical demand change as external barbell load increases. Using a computational framework that integrates kinematic motion generation with nonlinear moment-limited joint mechanics, mechanically admissible squat trajectories were reconstructed for different loading conditions.

The numerical simulations demonstrate that increasing barbell load leads to systematic adaptations of squat posture. In particular, heavier loads produce a posterior displacement of the pelvis and increased forward inclination of the torso. These changes reduce the mechanical demand on the knee joint while transferring a larger portion of the rotational load to the hip joint. The results therefore indicate a gradual transition toward a more hip-dominant movement pattern as the external load increases.

 doi:10.20944/preprints202603.1923.v1

The predicted joint moment distributions further show that the hip and knee joints operate closest to their mechanical limits during the deepest phase of the squat, while the ankle joint remains comparatively less critical. These findings highlight the importance of joint strength constraints in determining mechanically feasible squat techniques under heavy loading.

Overall, the presented results demonstrate that the interaction between body geometry, external load, and joint moment capacity plays a central role in shaping squat mechanics. The proposed computational approach provides a useful tool for analyzing load-dependent movement adaptations and may support future research in biomechanics, sports science, and strength training analysis.

Author Contributions: Conceptualization, K.N.; methodology, K.N., A.S.-G. and T.G.; software, K.N. and T.G.; validation, K.N., A.S.-G., A.C. and T.G.; formal analysis, K.N.; investigation, K.N.; resources, K.N. and A.C.; data curation, K.N. and A.C.; writing—original draft preparation, K.N.; writing—review and editing, A.S.-G., A.C. and T.G.; visualization, K.N. and T.G.; supervision, A.S.-G. and T.G.; project administration, A.S.-G. and T.G.; funding acquisition, A.S.-G. and A.C. All authors have read and agreed to the published version of the manuscript.

Funding: This research received no external funding.

Institutional Review Board Statement: Not applicable.

Informed Consent Statement: Not applicable.

Data Availability Statement: The original contributions presented in this study are included in the article. Further inquiries can be directed to the corresponding author.

Conflicts of Interest: The authors declare no conflicts of interest.

References

1. Chandler, T.J.; Stone, M.H. The squat exercise in athletic conditioning: A position statement and review of the literature. *Strength Cond. J.* **1991**, *13*, 51–60.
2. Swinton, P.A.; Lloyd, R.; Keogh, J.W.L.; Agouris, I.; Stewart, A.D. A biomechanical comparison of the traditional squat, powerlifting squat, and box squat. *J. Strength Cond. Res.* **2012**, *26*, 1805–1816.
3. McLaughlin, T.M.; Dillman, C.J.; Lardner, T.J. A kinematic model of performance in the parallel squat by champion powerlifters. *Med. Sci. Sports Exerc.* **1977**, *9*, 128–133.
4. Escamilla, R.F.; Fleisig, G.S.; Lowry, T.M.; Barrentine, S.W.; Andrews, J.R. A three-dimensional biomechanical analysis of the squat during varying stance widths. *Med. Sci. Sports Exerc.* **2001**, *33*, 984–998.
5. Schoenfeld, B.J. Squatting kinematics and kinetics and their application to exercise performance. *J. Strength Cond. Res.* **2010**, *24*, 3497–3506.
6. McCaw, S.T.; Melrose, D.R. Stance width and bar load effects on leg muscle activity during the parallel squat. *Med. Sci. Sports Exerc.* **1999**, *31*, 428–436.
7. Paoli, A.; Marcolin, G.; Petrone, N. The effect of stance width on the electromyographical activity of eight superficial thigh muscles during back squat with different loads. *J. Strength Cond. Res.* **2009**, *23*, 246–250.
8. Signorile, J.F.; Kwiatkowski, K.; Caruso, J.F.; Robertson, B. Effect of foot position on the electromyographical activity of the superficial quadriceps muscles during the parallel squat and knee extension. *J. Strength Cond. Res.* **1995**, *9*, 182–187.
9. Hales, M.E.; Johnson, B.F.; Johnson, J.T. Kinematic analysis of the powerlifting style squat and the conventional deadlift during competition: Is there a cross-over effect between lifts? *J. Strength Cond. Res.* **2009**, *23*, 2574–2580.
10. Wretenberg, P.; Feng, Y.; Arborelius, U.P. High- and low-bar squatting techniques during weight-training. *Med. Sci. Sports Exerc.* **1996**, *28*, 218–224.
11. Brown, L.E.; Shepard, G.; Sjostrom, T. Performance box squats. *Strength Cond. J.* **2003**, *25*, 22–23.
12. Fry, A.C.; Smith, C.; Schilling, B.K. Effect of knee position on hip and knee torques during the barbell squat. *J. Strength Cond. Res.* **2003**, *17*, 629–633.
13. Chiu, L.Z.F.; Heiler, J.; Sorenson, S.C. Sitting back in the squat. *Strength Cond. J.* **2009**, *31*, 25–27.

 doi:10.20944/preprints202603.1923.v1

14. Kawamori, N.; Rossi, S.J.; Justice, B.D.; Haff, E.E.; Pistilli, E.E.; O'Bryant, H.S.; Haff, G.G. Peak force and rate of force development during isometric and dynamic mid-thigh clean pulls performed at various intensities. *J. Strength Cond. Res.* **2006**, *20*, 483–491.
15. Cormie, P.; McCaulley, G.O.; Triplett, N.T.; McBride, J.M. Optimal loading for maximal power output during lower-body resistance exercises. *Med. Sci. Sports Exerc.* **2007**, *39*, 340–349.
16. Zink, A.J.; Perry, A.C.; Robertson, B.L.; Roach, K.E.; Signorile, J.F. Peak power, ground reaction forces, and velocity during the squat exercise performed at different loads. *J. Strength Cond. Res.* **2006**, *20*, 658–664.
17. Cronin, J.; Sleivert, G. Challenges in understanding the influence of maximal power training on improving athletic performance. *Sports Med.* **2005**, *35*, 213–234.
18. Wilson, G.J.; Murphy, A.J.; Pryor, J.F. Musculotendinous stiffness: Its relationship to eccentric, isometric, and concentric performance. *J. Appl. Physiol.* **1994**, *76*, 2714–2719.
19. Ireland, M.L. The female ACL: Why is it more prone to injury? *Orthop. Clin. North Am.* **2002**, *33*, 637–651.
20. Leetun, D.T.; Ireland, M.L.; Willson, J.D.; Ballantyne, B.T.; Davis, I.M. Core stability measures as risk factors for lower extremity injury in athletes. *Med. Sci. Sports Exerc.* **2004**, *36*, 926–934.
21. Kadaba, M.P.; Ramakrishnan, H.K.; Wooten, M.E. Measurement of lower extremity kinematics during level walking. *J. Orthop. Res.* **1990**, *8*, 383–392.
22. Gutierrez-Farewik, E.M.; Bartonek, A.; Saraste, H. Comparison and evaluation of two common methods to measure center of mass displacement in three dimensions during gait. *Hum. Mov. Sci.* **2006**, *25*, 238–256.
23. Stone, M.H.; Hornsby, W.G.; Mizuguchi, S.; Sato, K.; Gahreman, D.; Duca, M.; Carroll, K.M.; Ramsey, M.W.; Stone, M.E.; Pierce, K.C.; et al. The use of free weight squats in sports: A narrative review—Terminology and biomechanics. *Appl. Sci.* **2024**, *14*, 1977. https://doi.org/10.3390/app14051977
24. Escamilla, R.F.; Fleisig, G.S.; Zheng, N.; Lander, J.E.; Barrentine, S.W.; Andrews, J.R.; Bergemann, B.W.; Moorman, C.T. Effects of technique variations on knee biomechanics during the squat and leg press. *Med. Sci. Sports Exerc.* **2001**, *33*, 1552–1566.
25. McBride, J.M.; Skinner, J.W.; Schafer, P.C.; Haines, T.L.; Kirby, T.J. Comparison of kinetic variables and muscle activity during a squat vs. a box squat. *J. Strength Cond. Res.* **2010**, *24*, 3195–3199.
26. Pereira, G.R.; Leporace, G.; Chagas, D.V.; Furtado, L.F.L.; Praxedes, J.; Batista, L.A. Influence of hip external rotation on hip adductor and rectus femoris myoelectric activity during a dynamic parallel squat. *J. Strength Cond. Res.* **2010**, *24*, 2749–2754.
27. Decker, M.; Krong, J.; Peterson, D.; Anstett, T.; Torry, M.; Giphart, E.; Shelburne, K.; Philippon, M. Deep hip muscle activation during a squat exercise. In *Proceedings of the American Society of Biomechanics*; PA, USA, 2009.
28. Wu, H.; Lee, S.; Kao, J.; Wang, S. Three-dimensional kinetic analysis of lower limbs in barbell squat. In *Proceedings of the 37th Annual Northeast Bioengineering Conference*; Rochester, NY, USA, 2011.
29. Swinton, P.A.; Lloyd, R.; Agouris, I.; Stewart, A. Contemporary training practices in elite British powerlifters: Survey results from an international competition. *J. Strength Cond. Res.* **2009**, *23*, 380–384.
30. American College of Sports Medicine. Progression models in resistance training for healthy adults. *Med. Sci. Sports Exerc.* **2009**, *41*, 687–708.